Atmos. Chem. Phys. Discuss., 12, 19209–19241, 2012
www.atmos-chem-phys-discuss.net/12/19209/2012/
doi:10.5194/acpd-12-19209-2012

Atmospheric Chemistry and Physics Discussions

Global mapping of vertical injection profiles of wild-fire emission

M. Sofiev[1], **R. Vankevich**[2], **T. Ermakova**[2], **and J. Hakkarainen**[3]

[1]Finnish Meteorological Institute, Helsinki, Finland
[2]Russian State Hydrometeorological University, St. Petersburg, Russia
[3]Lappeenranta University of Technology, Lappeenranta, Finland

Received: 9 July 2012 – Accepted: 16 July 2012 – Published: 2 August 2012

Correspondence to: M. Sofiev (mikhail.sofiev@fmi.fi)

Published by Copernicus Publications on behalf of the European Geosciences Union.

Abstract

A problem of a characteristic vertical profile of smoke released from wild-land fires is considered. A methodology for bottom-up evaluation of this profile is suggested and a corresponding global dataset is calculated. The profile estimation is based on: (i) a semi-empirical formula for plume-top height recently suggested by the authors, (ii) MODIS satellite observations of active wild-land fires, and (iii) meteorological conditions evaluated at each fireplace using output of ECMWF weather prediction model. Plumes from all fires recorded globally during two arbitrarily picked years 2001 and 2008 are evaluated and their smoke injection profiles are estimated with a time step of 3 h. The resulting 4-dimensional dataset is split to day- and night-time subsets. Each of the subsets is projected to global grid with resolution $1^{\circ} \times 1^{\circ} \times 500$ m, averaged to monthly level, and normalised with total emission. Evaluation of the obtained dataset was performed at several levels. Firstly, the quality of the semi-empirical formula for plume-top computations was evaluated using recent additions to the MISR fire plume-height dataset. Secondly, the obtained maps of injection profiles are compared with another global distribution available from literature. Thirdly, the upper percentiles of the profiles are compared with an independent dataset of space-based lidar CALIOP. Finally, the stability of the calculated profiles with regard to inter-annual variations of the fire activity and meteorological conditions is roughly estimated by comparing the sub-sets for 2001 and 2008.

1 Introduction

Wild-land fires is one of the major contributors of trace gases and aerosols to the atmosphere. The fire smoke affects chemical and physical properties of the atmosphere at a wide range of spatial and temporal scales, which are directly related to lifetime of the released pollutants in the atmosphere. The species lifetime is determined by the removal and chemical transformations processes, which strongly depend on altitude. The

ACPD
12, 19209–19241, 2012

bulk of the fire smoke is released in the atmospheric boundary layer (ABL) (Val Martin et al., 2010; Sofiev et al., 2009, 2012) but strong fires occurring under favourable atmospheric conditions can send the plumes high into the free troposphere (FT) (Freitas et al., 2007; Labonne et al., 2007) and up to the stratosphere, where the smoke can stay for long time and spread over very wide areas (Dirksen et al., 2009; Fromm et al., 2000; Luderer et al., 2006). Therefore, it is of crucial importance for both climate and atmospheric composition applications to reproduce the vertical profiles of the fire plumes.

Most atmospheric composition models distribute the fire emissions homogeneously starting from the ground up to a prescribed plume-top height H_p, which is sometimes region-dependent. For global chemistry-transport models, Davison (2004), Forster et al. (2001), and Liousse et al. (1996) set it to about 2 km, whereas for regional simulations of smoke from intense Canadian fires Westphal and Toon (1991) used 5–8 km. Lavoué et al. (2000) showed that H_p is usually about 2–3 km for fires in the northern latitudes, but can reach 7–8 km for powerful crown fires. Biomass burning in Central America is usually less intense, therefore $H_p \sim 0.9$–1.5 km was suggested by Kaufman et al. (2003) for that region. Following this estimation, Wang et al. (2006) used 1.2 km (8th model layer) in mesoscale simulations and conducted sensitivity studies showing 15 % variation of the near-surface concentrations if H_p is varied plus-minus one model layer (a few hundreds of meters).

More accurate approaches for the fire injection height computations suggested by Freitas et al. (2007), Lavoué et al. (2000), and Sofiev et al. (2012) are based on explicit accounting for the features of individual fires and actual ambient atmospheric conditions. These methods provide better representation of the plume vertical distribution but share the same weakness: application of the methodologies requires quite detailed information on each fire. This information is not available if the emission estimates are based on burnt-area data or are aggregated in time and space (e.g. the widely used Global Fire Emission Dataset GFED, van der Werf et al., 2006). Therefore, there is a need for pre-calculated "climatologic" injection profile of wild-land fires emission, which

ACPD
12, 19209–19241, 2012

can be used in practical applications if the detailed fire information is not available or too bulky.

An estimation of typical injection height from fires for Northern America was performed by Val Martin et al. (2010) using MISR plume height observations. The authors have evaluated the inter-annual variability, relation to vegetation type, as well as seasonal variations of the smoke injection height using statistics of about 3300 plumes. Dentener et al. (2006) suggested a single global map of the injection top height but did not specify the underlying data and analytic procedures.

The goal of the current work is to estimate the characteristic injection vertical profiles of the wild-land fire plumes over the globe, to determine its diurnal and seasonal variations, and to estimate peculiarities of their spatial distribution patterns.

In the following section we outline the input methodology, formalise the problem and describe the input datasets; Sect. 4 describes the preparatory steps and additional evaluation of the methodologies involved. Section 5 presents the outcome of the calculations, whereas Sect. 6 compares it with other datasets and discusses some features of the obtained profiles.

2 Materials and methods

2.1 Calculation of top-height of the fire emission plumes

Calculation of the characteristic injection profile is based on recently suggested semi-empirical formula for the fire-plume top height (Sofiev et al., 2012). According to this methodology, the plume-top H_p depends on the Fire Radiative Power FRP, height of the atmospheric boundary layer ABL H_{abl}, and Brunt-Vaisala frequency in the free troposphere N_{FT}:

$$H_p = \alpha H_{abl} + \beta \left(\frac{FRP}{P_{f0}}\right)^{\gamma} \exp(-\delta N_{FT}^2/N_0^2) \quad (1)$$

ACPD
12, 19209–19241, 2012

Coefficients α, β, γ, and δ, and normalising constants P_{f0} and N_0 are:

$$\alpha = 0.24; \beta = 170\,\mathrm{m}; \gamma = 0.35; \delta = 0.6; P_{f0} = 10^6 W; N_0^2 = 2.5 \times 10^{-3}\mathrm{s}^{-2} \quad (2)$$

2.2 Determination of characteristic vertical profile of fire emission

Problem statement

Let intensities of fires $[f_i,\ i = 1..N_f]$ be observed by a satellite instrument when the spacecraft overpasses the burning area at times $[\tau_j,\ j = 1..N_\tau]$. The result of the observation is recorded as a radiation power $P_{fi}\ (\tau_j)$ for each fire f_i and overpass time τ_j. Let meteorological data be available from a meteorological model as time- and space-dependent variables: ABL height $H_{ABL}(x,y,t)$, and the FT Brunt-Vaisala frequency $N^2(x,y,z,t)$.

The goal is to evaluate the gridded monthly-mean vertical distribution of the fire emission:

$$e(i,j,k,m);\ i = \overline{I,I};\ j = \overline{I,J};\ k = \overline{I,K};\ m = \overline{1,12};\ \sum_{k=1}^{K} e(i,j,k,m) = 1,\ \text{for each } i,j,m \quad (3)$$

where I,J,K are the x-, y-, and z-wise dimensions of the grid, i,j,k are corresponding indices, and m is month number.

The analysis is to be performed separately for day- and night-time injection.

Problem solution

Following Sukhinin et al. (2005), Kaufman et al. (1998), and (Sofiev et al., 2009), we assume a linear relation of the fire intensity P_f [W] and its emission rate E [$\mathrm{kg\,s^{-1}}$]. It leads to the following distribution of the emitted species during the lifetime τ of the fire f:

$$e_f(x_f, y_f, z) = s_e(x_f, y_f) \int_\tau P_f(t) P_f(t) \varepsilon(H_p(t), z) \mathrm{d}t \quad (4)$$

ACPD
12, 19209–19241, 2012

where s_e is emission factor converting P_f to the emission rate of particular species, x_f and y_f are the fire coordinates, H_p is given by the Eq. (1), and ε [kg s^{-1} m^{-1}] is vertical profile of emission from individual fire, which is assumed to have the same shape for all fires and dependent only on the plume top height H_p.

For determination of ε, following Briggs (1975), the plume thickness is taken equal to height of its centreline H_C, so that $H_p = 1.5H_C$. Distribution of the emitted masses is then taken homogeneous from $H_p 3^{-1}$ up to H_p.

Having the emission distribution from a single fire Eq. (4) computed for all fires, the needed monthly gridded distribution in each grid cell (i, j) can be obtained via summation over all fires f_m (i, j) that occurred within its borders during each month m. For the vertical layer k, which extends from $z_{k-1/2}$ till $z_{k+1/2}$, finally obtain:

$$e(i,j,k,m) = \frac{\int_{z_{k-1/2}}^{z_{k+1/2}} \sum_{f_m(i,j)} e_f(x_f, y_f, z)\mathrm{d}z}{\int_{0}^{\infty} \sum_{f_m(i,j)} e_f(x_f, y_f, z)\mathrm{d}z} \quad (5)$$

The simplest case considered further is computation of vertical distribution for the total fire emission (sum over all species). According to Sukhinin et al. (2005), the fire radiative energy release is linearly connected with the burnt fuel and, following Kaufman et al. (1998), with the total amount of the released trace gases and aerosols. For such a case, the emission factor s_e is independent from the land-use type and therefore is cancelled out during the normalization step Eq. (5).

For individual species the emission factor s_e is land-use and fire-type dependent. It also varies for different stages of a fire lifecycle, which makes the consideration of the full integral Eq. (4) inevitable. As a result, the mean distribution will be specific for each species. Corresponding emission factors can be taken from the Integrated System for wild-land fires (IS4FIRES, Sofiev et al., 2009) for total PM and re-scaled to other species following Andreae and Merlet (2001). However, with limited fire information

ACPD
12, 19209–19241, 2012

available and large uncertainties of the methodologies and all empirical coefficients, this extra complexity of the computations is not justified. Therefore, below the profiles were computed for total emission only.

2.3 Input data for the computations

2.3.1 Fire intensity data

The information on the wild-land fires intensity needed for the above procedure is obtained from the active-fire observations by Moderate Resolution Imaging Spectroradiometer (MODIS) instrument onboard Aqua and Terra satellites (http://modis.gsfc.nasa.gov; Justice et al., 2002; Kaufman et al., 1998). The MODIS collection 5 of the active fire characteristics includes release rate of radiative energy from overheated pixels, the Fire Radiative Power (FRP, [W]). This dataset is the only existing collection that covers the whole globe over more than a decade and provides characteristics of active fires.

FRP products have recently become available also from geostationary satellites, such as the Spinning Enhanced Visible and Infrared Imager (SEVIRI; Kaiser et al., 2009; Roberts and Wooster, 2008) onboard of Meteosat MSG satellite. Large pixel size of such satellites (more than $10 \times 10\,km^2$) precludes their direct utilization since such pixel often covers many individual fires. However, high temporal resolution (15 min for SEVIRI) makes them a valuable source of information about the temporal evolution of the fire intensity.

2.3.2 Meteorological parameters

The meteorological information over the globe is taken from the operational archives of the Integrated Forecasting System (IFS) of European Centre for Medium-Range Weather Forecast (ECMWF, http://www.ecmwf.int). The Brunt-Vaisala frequency was computed from vertical temperature profile. The ABL height was estimated by the

ACPD
12, 19209–19241, 2012

dry-parcel method, whose performance was evaluated and compared with other approaches by Sofiev et al. (2006) and Fisher et al. (1998).

2.3.3 Plume height and profile observations

The plume-top formulations Eqs. (1)–(2) have been evaluated by Sofiev et al. (2012) for boreal and mid-latitude fires, which is insufficient for the purposes of this work. Therefore, additional evaluation was performed using the new observations of the Multi-angle Imaging SpectroRadiometer (MISR) Plume Height Project (Kahn et al., 2008; Mazzoni et al., 2007). For the current study we used all information available to-date, which included injection heights for about 2500 fires that took place in the US, Canada, Siberia, Africa, and Borneo during 2005–2009.

An independent evaluation of the obtained mean vertical profiles was performed using the new space lidar dataset of Cloud-Aerosol Lidar with Orthogonal Polarization (CALIOP) onboard of NASA CALIPSO satellite (CALIPSO, 2011a). The dataset is a globally-gridded monthly product derived from the CALIOP level 2 aerosol profiles (Vaughan et al., 2009a).

3 Preparatory steps for the profile calculations

Before starting the computations, several preparations have to be made: (i) additional evaluation of the plume-rise formula, (ii) development of a method for determination of the temporal evolution of the fire intensity, and (iii) selection of the method for filling-in the gaps in the obtained dataset.

3.1 Global evaluation of the plume rise formula

The global-scale evaluation of the formulations Eqs. (1)–(2) is based on new MISR data, which were not available for the original study (Sofiev et al., 2012). The new datasets for Africa and Borneo allow extending the original boreal- and

ACPD
12, 19209–19241, 2012

temperate-forest evaluation towards savannah and tropical forests. We considered only so-called "good" plume height retrievals, for which the accuracy of the plume-top retrieval is the highest. This selection reduces the size of the dataset from about 2500 fire cases down to 1650 cases, which is sufficient for the task.

The comparison of predictions of formulas Eqs. (1)–(2) with MISR observations (Fig. 1) confirms (and even strengthens) the main conclusion of the original evaluation by Sofiev et al. (2012). The parameterization is capable of predicting the top height of >70 % of the fire plumes within 500 m from the MISR observations. For Borneo the fraction of good predictions was even higher: 94 %. Therefore, the formulations Eqs. (1)–(2) can be used over the whole globe. Some details of the formula performance are further discussed in Sect. 7.

3.2 Diurnal cycle of fire intensity

During night, both fire intensity and turbulent mixing are suppressed, which leads to reduction of the number of active fires N_{fires} and mean FRP per active fire $\text{FRP}_{\text{per-fire}}$. Their product, total regional $\text{FRP}_{\text{total}}$, decreases even stronger, which corresponds to low night-time emission. The diurnal cycle of $\text{FRP}_{\text{per-fire}}$ contributes to that of the injection height – together with the night-time stable atmospheric stratification and low ABL height. The goal of this preparatory step is therefore to obtain diurnal cycles of $\text{FRP}_{\text{total}}$ and $\text{FRP}_{\text{per-fire}}$, which would be compatible with MODIS active-fire observations.

Estimating of diurnal cycles directly from MODIS data is not feasible. Four overpasses per day, even if not obscured by clouds, are not sufficient to resolve this cycle (Ichoku et al., 2008). One has to use instruments at geostationary orbit (GEO), which temporal resolution (∼15 min) is sufficiently high to estimate diurnal variations of both $\text{FRP}_{\text{total}}$ and $\text{FRP}_{\text{per-fire}}$ (Roberts and Wooster, 2008; Roberts et al., 2009). The only LEO satellite, which has more than 10 overpasses per day over equatorial region, is TRMM with Visible and Infrared Scanner VIRS onboard, which provides active-fire counts. Using VIRS, Giglio (2007) estimated the variation of the number of active fires for LEO data, which appeared about as large as that found by Roberts et al. (2009)

ACPD
12, 19209–19241, 2012

for SEVIRI. Analysis of FRP could not be performed due to early saturation of VIRS infrared channels.

Comparing the results for SEVIRI and VIRS, we concluded that derivation of diurnal cycle of $FRP_{per\text{-}pixel}$ (the closest available analogy of $FRP_{per\text{-}fire}$) for LEO satellite seems to be beyond the reach: the uncertainties and scatter in the data are too high. However, the dynamic range of the variation of the number of fires reported for TRMM and SEVIRI appeared comparable, suggesting that SEVIRI-based variation of $FRP_{per\text{-}pixel}$ would be sufficient for the present study.

Since none of the above works provided quantitative characteristics of the variations, the analysis was repeated for complete 2010 for the whole SEVIRI domain for both FRP_{total} and $FRP_{per\text{-}pixel}$ variations (Table 1 and Fig. 2). The former was used to simulate the diurnal cycle of emission fluxes, whereas the latter was used for the injection height. Both variations were used without separation of the land use types: from large SEVIRI pixels it was not possible to distinguish between the fires that would shut down in the evening from those that will survive throughout night. We had to apply the corresponding mean variations to all fires, thus ignoring the vegetation type. Owing to similarity of the profiles for different land-use classes (Fig. 2) and foregoing spatial averaging to $1^\circ \times 1^\circ$ grid, the extra uncertainty is believed to be small.

3.3 Gap closure and spatial smoothing

The bottom-up approach of the profile computations, being potentially the most-accurate, has a drawback: there are areas where few or no fires took place during some months of the analysed years (Fig. 3). To reduce its impact, a gap-filling procedure is needed.

The gap-filling is applied to the cells, which have no fires during the specific period but have at least 3 out of 8 neighbouring cells with normally computed profiles: $N_{valid} \geq 3$. Then the profile in the empty cell (i_e, j_e) for the month m_e is a linear combination of the valid neighbouring ones (i_n, j_n), weighted with the number of fires N_{fn} in

ACPD
12, 19209–19241, 2012

each of them:

$$e(i_e, j_e, k, m_e) = \frac{\sum_{n=1}^{N_{valid}} e(i_n, j_n, k, m_e) N_{fn}(i_n, j_n, m_e)}{\sum_{n=1}^{N_{valid}} N_{fn}(i_n, j_n, m_e)}, \; k = \overline{1, K} \quad (6)$$

An optional spatial smoothing procedure can be useful for low-resolution global simulations, which cannot handle quickly varying input fields. In the current study, it was realised via 27-point 3-D running average over valid immediate neighbours of each grid cell (i_f, j_f, k_f) for all months:

$$e(i_f, j_f, k, m_f) = \frac{1}{N_{val3D}} \sum_{n=1}^{N_{val3D}} e(i_n, j_n, k_n, m), \; m = \overline{1, 10} \quad (7)$$

Here the averaging set is composed of the grid cell (i_f, j_f, k_f) and its 26 immediate neighbours. Only valid cells are included, thus $1 \le N_{val3D} \le 27$.

The running averaging, being an efficient smoother, also artificially reduces the variability between the cells with different features of the fires. Therefore, below the results are presented without this step. The numerical dataset, however, includes the profiles both before and after the smoothing.

4 Results

The results of the computations consist of 12 monthly 3-D distributions of the fire emission over the globe, separately for day and night time (http://is4fires.fmi.fi). Spatial pattern of injection heights appeared to be comparatively homogeneous at regional level but differences between the regions are substantial. In particular, there are several clearly identifiable areas with particularly low and particularly high fires (Fig. 4).

ACPD
12, 19209–19241, 2012

The highest plumes are predicted for forested regions of Northern America (Rocky Mountains), part of Middle East to the south of Caspian Sea, and Australia. During local summer season in these regions, the 50th percentile of mass injection profile exceeds 3 km, whereas the 90th percentile is higher than 4 km (i.e. 50 % and 90 % of mass is emitted inside the layer spanning from the surface up to > 3 km and > 4 km, respectively).

Regions with comparatively high injection are forests in Amazonia and equatorial Africa, as well as grasses in southern Africa and central Eurasia. There, the 50th percentile is generally confined within 2.5 km, whereas 90 % of mass stays within 3 km.

Among the regions with generally low injection, one can mention densely populated regions in all continents. There, the fires are probably better controlled and thus do not reach the strength needed to send the smoke high up in the atmosphere. Interestingly, the infamous extremely high plumes from Siberian and Alaskan fires did not manifest themselves in the profiles in those regions during the considered period. Possibly, there were no such fires during the considered two years – or they were overshadowed by numerous moderate episodes that are much more frequent and are responsible for the bulk of annual emission.

Seasonal variation of the profiles largely follow the fire season (Fig. 4). In temperate and boreal climate, the highest injection occurred during local summer, whereas fires in tropical regions mainly occur during dry season. Thus, in equatorial Africa, it is February for the regions to the north of equator and August for areas to the south of it that are characterised by the highest injection.

In general, the results agree with general expectations that the strong fires are more probable in the areas with the highest fuel load, strong droughts, and poor forest and fire management. Zonally-averaged vertical profile (Fig. 5) shows a similar picture: in the equatorial region, where the bulk of contribution is from comparatively wet equatorial forests (predominantly man-made fires), the top of the injection profile is lower than in the drier middle latitudes. One can also see that, despite the record-high fires can bring the top of profile above 6 km, they have little impact to the bulk of the emission:

ACPD
12, 19209–19241, 2012

globally, more than 50 % of the fire emission is confined with in the lowest 1–2 km, i.e. within the ABL.

Figure 5 also highlights the impact of diurnal variation of both fire intensity and boundary layer height. These quantities vary synchronously: small fires and shallow boundary layer lead to low injection during night, whereas stronger fires and deeper ABL during day result in significantly higher injection. As a zonal mean, the bulk of emission during night is confined within 500 m, whereas during day it spreads up to 1.5–2 km.

5 Discussion

5.1 Quality of the plume-top prediction formula

Additional evaluation of the plume-top formulations Eqs. (1)–(2) has confirmed high accuracy of the approach but also highlighted the tendency of the parameterization to over-state the height of low plumes and under-estimate the high ones. For the African dataset this resulted in a high bias of ~ 150 m, owing to significant fraction of over-stated low plumes ($H_p < 700$ m). For Borneo, where the fires were more powerful and plumes generally went from 700 m to 1.5 km, the agreement was very good: bias was less than 30 m and > 90 % of the plumes were predicted within 500 m from the observations.

A potential explanation of this tendency is that the grass fires usually occupy wide areas, so that the FRP density, [W m^{-2}], is substantially lower than that for the forest fires – despite the total FRP can be comparable. The present formulations do not take this into account due to high uncertainty of the fire area estimations and practically unknown fire shape (position of the fire fronts, temperature distribution over the burn area, etc.). As a result, predicted plume top for a wide but low-FRP-density fire will be the same as that for a concentrated limited-area event – providing that the total FRPs

ACPD
12, 19209–19241, 2012

and meteorological conditions are the same. In reality, one might expect the plume from a concentrated fire to be injected higher.

Similar dependence of the plume injection height on the fire area was noticed by Raffuse et al. (2012), where the plume-rise parameterization experienced difficulties for the very wide fires in the north-western US.

The other uncertainty of the approach is connected with a time period needed for the plume to reach its top position. Since MISR and MODIS are both onboard of Terra satellite, their observations are performed simultaneously. However, the observed plume is formed by smoke released from the fire some 15–30 min before the overpass. Consequently, the height of the plume should also be related to the past-time FRP. In the morning and evening hours, it can lead to up to 20–30 % of difference in the FRP value (if estimated from the parameters of Table 1), i.e. can bring a few tens of metres of difference to the H_p prediction.

5.2 Representativeness of the obtained profiles for individual episodes

The current profiles have been obtained from the analysis of two distant years – 2001 and 2008. These two years provided sufficient coverage ensuring that no region is missed from the maps (Figs. 3 and 4). Still, the number of fire events for specific months can be fewer than 10 for about 10–20 % of grid cells (Fig. 3). For these areas the results of the current computations should be taken with care.

A rough estimation of representativeness of the obtained results can be derived from comparison of the results for individual years (Fig. 6). One can see that the main patterns are repeated in both years. At the same time, particularly strong or weak fire season over some area can have significant regional impact. Thus, strong fires in 2008 in Middle East resulted in sharply higher injection there. That year also appeared somewhat stronger in Amazonia and Eastern US although the difference is more randomly distributed. In Europe, injection height in 2001 was slightly higher whereas in Oceania and Australia the difference is small.

ACPD
12, 19209–19241, 2012

In general, the difference mainly stays within 500 m but can exceed 1 km in some grid cells.

Apart from the inter-annual variability, one should also keep in mind that in 2001 the fire information was coming from only one satellite Terra. As a result, observations of, for instance, African fires were only in the morning and evening, whereas Aqua (launched in 2002 and thus contributed to 2008 dataset) has a mid-day and mid-night overpasses. Therefore, uncertainties of the diurnal variation may have contributed to the difference between the years.

5.3 Diurnal and seasonal variations of the injection profiles

Diurnal variation of the injection height is huge (Fig. 5): practically, one can consider two independent datasets – one for daytime and one for nighttime, with transition during morning and evening. A variable controlling this transition can be ABL height or sun zenith angle. Both these quantities correlate well with FRP and plume injection height.

Apart from the diurnal variations, the seasonal changes of the injection profile are also important: both FRP and ABL height follow quite similar seasonal curves with peaks in dry hot months. As a result, the mean height of, for instance, the 90th percentile of the injection profiles shows seasonal variation about 30–40 %. This result is in qualitative agreement with Val Martin et al. (2010) estimates for Northern America.

Correlation of ABL top and plume injection heights leads to fairly constant fraction of the fire smoke emitted inside the ABL: about 50 %. This fraction agrees well with statistics of (Val Martin et al., 2010) and can also be related to the 85 % of the total number of fire plumes confined inside the ABL (Sofiev et al., 2009). Comparing these fractions, one can conclude that 15 % of the most-powerful fires bring ∼50 % of the smoke emission into the free troposphere – and this fraction stays comparatively constant throughout the year. Difference of the ABL emission fraction between day and night is somewhat larger but the scatter is very wide, so it is difficult to provide quantitative estimates. In-average, one can use the ABL-injected fraction of 50–60 % as a rough estimate.

ACPD
12, 19209–19241, 2012

5.4 Comparison with CALIOP observations

Recently developed product of CALIOP space-based lidar provides monthly vertical profiles of aerosols (CALIPSO, 2011b). The instrument is capable of detecting the features of the aerosols. In many cases, it can also guess their origin (Vaughan et al., 2009b). For evaluation purposes, we selected only profiles marked as fire-originated (Fig. 7).

Direct comparison between the profiles obtained in the present work and the CALIOP observations is not possible because the underlying fire episodes are very different: (i) CALIOP observes less than 3 % of the earth surface and its overpasses are infrequent, (ii) it cannot distinguish between fresh and aged plumes, (iii) detection of the plume type is not always accurate. However, the upper percentiles of injection height can still be compared over regions with widespread fires – see Fig. 4 (right-hand panels) and Fig. 7.

The CALIOP 90th percentile maps for February (Fig. 7a) are quite sparse. The typical height in the Southern Europe seems to be between 1km and 1.5 km, which is the same range as in the present study (Fig. 4b), with somewhat wider areas with above-1 km plumes. In the South-East Asia, the pattern is very irregular ranging from less than 1 km up to 4 km heights, whereas the current study suggested quite homogeneous 1–2 km elevation. No fire plumes were recognised by CALIOP in equatorial Africa, whereas in the south their density is disproportionally large compared to that of active fires (the main fire season there is in June–September, not February). These inconsistencies are probably due to incorrect attribution of the observed plumes. Still, the main pattern in Southern Africa qualitatively coincides with our results: the 90th percentile of the plumes is between 1 and 3 km with downward trend towards the eastern coast. Finally, sparse observations in Southern America suggest about 1.5 km typical height, also in agreement with current predictions.

Comparison of the patterns for August is more conclusive: plumes in Amazonia, Southern Africa, Southern Europe and, to a less extent, Eastern US and South-East

ACPD
12, 19209–19241, 2012

Asia, are represented in the CALIOP dataset. Similarly to February, the ranges are similar to the present study with a tendency to show higher elevations than predicted – by a few hundreds of metres.

The limited but systematic difference between our estimates and CALIOP observations (current study predicts somewhat lower height of the 90th percentile) can originate from the uncertainties of our procedures or from aged plumes recorded by CALIOP together with fresh ones. Old plumes are dispersed over thicker layers, so that their top (and upper percentiles) is usually positioned higher. The impact of this mixture is well seen in Africa (Fig. 7b), where the plume elevation sharply increases with distance from burning areas – towards coastlines and offshore.

The impact of aged plumes made evaluation of the night-time profile meaningless: CALIOP did not record any significant difference compared to daytime, which is evidently incorrect. In several regions, the night-time plumes were claimed to be even higher than during day. This, however, is not surprising: the fire emission during day is much stronger than during night, so that the previous-day plumes recorded at night easily overshadow the fresh smoke and hide the actual position of the newly released plumes.

5.5 Comparison with AEROCOM

We are aware about only one spatially-resolving map of mean injection top, which is recommended for the AEROCOM (Aerosol Comparisons between Observations and Models) modelling community by Dentener et al. (2006). In that work, the authors assumed certain release profiles to the specific land-use types (see Table 4; Dentener et al., 2006) and suggested the maximum release height (see Fig. 8 adapted from Fig. 9 of Dentener et al., 2006). Unfortunately, the authors did not explain how the profiles and maximum heights were obtained.

The suggested AEROCOM maximum heights can be related to our upper percentile maps (Fig. 4), whereas the profiles of Table 4 of Dentener et al. (2006) can, to some

ACPD
12, 19209–19241, 2012

extent, be related to the zonal average (Fig. 5). Such comparison reveals some similarities but also significant differences between the estimates.

Among the similarities, one can notice the western part of Northern America, where both datasets suggest quite high fires routinely reaching 3 km and, according to the present study, exceeding this level. Agreement exists also over Oceania and part of Australia, where the height of 90 % of the mass injection is close to the top height recommended for AEROCOM.

For Southern America the datasets show significantly different patterns: the current assessment has not registered high plumes over the eastern coast and in the south, instead reporting them in the forest regions in the middle of the continent. With no independent estimates available for the region, it is hard to select one of the estimates. However, in the densely populated coastal regions the wild-land fires should be controlled tighter than in sparsely inhabited tropical forest. As a result, the fire strength should decrease in the denser populated regions. The number of fires follows this trend (Fig. 3), which indirectly supports that consideration and agrees with the pattern obtained in the present study.

Patterns over Eurasia and Australia differ strongly between the studies. The highest plumes in the AEROCOM map are over semi-desert areas of Australia and tundra in Northern Eurasia. According to MODIS, there were no fires at all registered there during the considered years. These regions are also characterised by low fuel load and, in case of Northern Eurasia, frequent occasions of thin boundary layer. Therefore, it seems unlikely to have particularly high plumes over these regions.

Difference exists also for Scandinavia and Lapland, where the AEROCOM map suggested very high plumes. However, the rare fires in those regions do not release the smoke high above the ground. The forests are closely monitored and maintained there, so that the fires are quickly extinguished. Also, even in summertime, the low ABL heights are quite frequent in boreal regions, which also suppresses the plume rise. Our analysis for that region showed typical injection under 2 km but the number of fires was small.

ACPD
12, 19209–19241, 2012

Comparison of zonal-mean profiles (example in Fig. 5) with latitude bands of Table 4, (Dentener et al., 2006) showed little common between the datasets. For the tropical latitude band (30° S–30° N), 1 km suggested by AEROCOM can be considered as a practical top of injection only during night-time (still with some 10–15 % of mass injected higher). During daytime, it raises to about 2.5 km. For temperate band (30° S–N–60° S–N), the 2 km level is too high for the night-time emission and too low for daytime. Finally, there is no high injection (up to 3–6 km) in the boreal regions of the Northern Hemisphere: fires there are predominantly of low intensity and injection height.

6 Summary

The presented dataset is the result of bottom-up computations of characteristic vertical profiles of smoke from wild-land fires. It is obtained by processing the records of active fires of MODIS instrument onboard of Aqua and Terra satellites. The analysis was made for day and night time separately, covered years 2001 and 2008, extended over the whole globe, and resulted in monthly 3-D maps of injected fraction of the fire smoke.

The computations showed that the highest plumes reaching up to 6–8 km are characteristic for forested areas, whereas grassland fires usually emit within the lowest 2–3 km. Over the globe, about 50 % of the fire emission is injected within the lowest 2 km, i.e. inside the atmospheric boundary layer.

Strong diurnal and seasonal variations of the injection profiles were found all over the globe. It is therefore recommended to account for these variations in practical applications.

Comparison with the independent CALIOP observations showed similar patterns. Somewhat higher altitude of the 90th percentile obtained by the lidar (a few hundreds of metres) could originate from the impact of aged plumes dispersed over thicker layers and recorded by the lidar together with the fresh smoke from the fires.

ACPD
12, 19209–19241, 2012

Comparison with AEROCOM dataset showed both similarities and differences between the injection height maps. However, in most cases the results of the current study seem to be more logical, especially in the areas with significant seasonal variations of the injection height.

Noticeable inter-annual variation and significant scatter over several regions suggest that dynamic evaluation of emission from each specific fire, if appears possible, would bring about more accurate estimates, especially if limited-time regional episode is concerned. Current dataset is mostly useful for long-term global and continental studies, where analysis of each individual fire is unfeasible.

The dataset is publicly available at http://is4fires.fmi.fi.

Acknowledgements. The study has been performed within the ESA GlobEmission and TEKES KASTU 2 projects. Support of EU FP7 PASODOBLE, PEGASOS, and Academy of Finland ASTREX and Russian Research project "Conducting of problem-oriented research in monitoring technologies and forecasting of atmospheric state in forest and peat fire". Discussions with MACC and AEROCOM fire assessment teams are highly appreciated. The MODIS, MISR and CALIOP satellite data were obtained from public online databanks of NASA. MSG SEVIRI data were archived from the ENVISAT dissemination service.

References

Andreae, M. O. and Merlet, P.: Emission of trace gases and aerosols from biomass burning, Global Biogeochem. Cy., 15, 955–966, 2001.

Briggs, G. A.: Plume rise predictions, in: Lectures on air pollution and environmental impact analyses, Boston, 59–111, 1975.

CALIPSO: CALIPSO Quality Statements Lidar Level 3 Aerosol Profile Monthly Products Version Release: 1.00, 2011a.

CALIPSO: CALIPSO Quality Statements Lidar Level 3 Aerosol Profile Monthly Products Version Release: 1.00, available at: http://eosweb.larc.nasa.gov/PRODOCS/calipso/Quality_Summaries/CALIOP_L3AProProducts_1-00.html, access: 10 June 2012, 2011b.

Davison, P. S.: Estimating the direct radiative forcing due to haze from the 1997 forest fires in Indonesia, J. Geophys. Res., 109, 1–12, doi:10.1029/2003JD004264, 2004.

ACPD

12, 19209–19241, 2012

Dentener, F., Kinne, S., Bond, T., Boucher, O., Cofala, J., Generoso, S., Ginoux, P., Gong, S., Hoelzemann, J. J., Ito, A., Marelli, L., Penner, J. E., Putaud, J.-P., Textor, C., Schulz, M., van der Werf, G. R., and Wilson, J.: Emissions of primary aerosol and precursor gases in the years 2000 and 1750 prescribed data-sets for AeroCom, Atmos. Chem. Phys., 6, 4321–4344, doi:10.5194/acp-6-4321-2006, 2006.

Dirksen, R. J., Folkert Boersma, K., de Laat, J., Stammes, P., van der Werf, G. R., Val Martin, M., and Kelder, H. M.: An aerosol boomerang: Rapid around-the-world transport of smoke from the December 2006 Australian forest fires observed from space, J. Geophys. Res., 114, 1–15, doi:10.1029/2009JD012360, 2009.

Fisher, B. E. A., Erbrink, J. J., Finardi, S., Jeannet, P., Joffre, S., Morselli, M. G., Pechinger, U., Seibert, P., and Thomson, D. J.: COST Action 710 – Final report, in: Harmonisation of the pre-processing of meteorological data for atmospheric dispersion models, edited by: Fisher, B. E. A., Erbrink, J. J., Finardi, S., Jeannet, P., Joffre, S., Morselli, M. G., Pechinger, U., Seibert, P., and Thomson, D., Office for Official Publications of the European Communities, Luxembourg, 431 pp., 1998.

Forster, C., Wandinger, U., Wotawa, G., James, P., Mattis, I., Althausen, D., Simmonds, P., O'Doherty, S., Jennings, S. G., Kleefeld, C., Schneider, J., Trickl, T., Kreipl, S., Jäger, H., and Stohl, A.: Transport of boreal forest fire emissions from Canada to Europe, J. Geophys. Res., 106, 22887–22906, doi:10.1029/2001JD900115, 2001.

Freitas, S. R., Longo, K. M., Chatfield, R., Latham, D., Silva Dias, M. A. F., Andreae, M. O., Prins, E., Santos, J. C., Gielow, R., and Carvalho Jr., J. A.: Including the sub-grid scale plume rise of vegetation fires in low resolution atmospheric transport models, Atmos. Chem. Phys., 7, 3385–3398, doi:10.5194/acp-7-3385-2007, 2007.

Fromm, M., Jerome, A., Hoppel, K., Hornstein, J., Bevilacqua, R., Shettle, E., Servranckx, R., Zhanqing, L., and Stocks, B.: Observations of boreal forest fire smoke in the stratosphere by POAM III, SAGE II, and lidar in 1998, Geophys. Res. Lett., 27, 1407–1410, doi:10.1029/1999GL011200, 2000.

Giglio, L.: Characterization of the tropical diurnal fire cycle using VIRS and MODIS observations, Remote Sens. Environ., 108, 407–421, doi:10.1016/j.rse.2006.11.018, 2007.

Ichoku, C., Giglio, L., Wooster, M. J., and Remer, L. A.: Global characterization of biomass-burning patterns using satellite measurements of fire radiative energy, Remote Sens. Environ., 112, 2950–2962, doi:10.1016/j.rse.2008.02.009, 2008.

ACPD
12, 19209–19241, 2012

Justice, C. O., Giglio, L., Korontzi, S., Owens, J., Morisette, J. T., Roy, D., Descloitres, J., Alleaume, S., Petitcolin, F., and Kaufman, Y.: The MODIS fire products, Remote Sens. Environ., 83, 244–262, 2002.

Kahn, R. A., Chen, Y., Nelson, D. L., Leung, F.-Y., Li, Q., Diner, D. J., and Logan, J. A.; Wildfire smoke injection heights: Two perspectives from space, Geophys. Res. Lett., 35, 4–7, doi:10.1029/2007GL032165, 2008.

Kaiser, J. W., Wooster, M. J., Roberts, G., Schultz, M. G., V. d. Werf, G., and Benedetti, A.: SEVIRI Fire Radiative Power and the MACC Atmospheric Services, in: EUMETSAT Meteorological Satellite Conf., EUMETSAT, Darmstadt, Germany, 2005–2009, 2009.

Kaufman, I., Steele, M., Cummings, D. L., and Jaramillo, V. J.: Biomass dynamics associated with deforestation, fire, and, conversion to cattle pasture in a Mexican tropical dry forest, Forest Ecol. and Manag., 176, 1–12, 2003.

Kaufman, Y. J., Justice, C. O., Flynn, L. P., Kendall, J. D., Prins, E. M., Giglio, L., Ward, D. E., Menzel, W. P., and Setzer, A. W.: Potential global fire monitoring from EOS-MODIS, J. Geophys. Res.-Atmos., 103, 32215–21238, 1998.

Labonne, M., Bréon, F.-M., and Chevallier, F.: Injection height of biomass burning aerosols as seen from a spaceborne lidar, Geophys. Res. Lett., 34, 1–5, doi:10.1029/2007GL029311, 2007.

Lavoué, D., Liousse, C., Cachier, H., Stocks, B. J., and Goldammer, J. G.: Modeling of carbonaceous particles emitted by boreal and temperate wildfires at northern latitudes, J. Geophys. Res., 105, 26871–26890, doi:10.1029/2000JD900180, 2000.

Liousse, C., Penner, J. E., Chuang, C., Walton, J. J., Eddleman, H., and Cachier, H.: A global three-dimensional model study of carbonaceous aerosols, J. Geophys. Res., 101, 19411–19432, doi:10.1029/95JD03426, 1996.

Luderer, G., Trentmann, J., Winterrath, T., Textor, C., Herzog, M., Graf, H. F., and Andreae, M. O.: Modeling of biomass smoke injection into the lower stratosphere by a large forest fire (Part II): sensitivity studies, Atmos. Chem. Phys., 6, 5261–5277, doi:10.5194/acp-6-5261-2006, 2006.

Mazzoni, D., Logan, J. A., Diner, D., Kahn, R. A., Tong, L., and Li, Q.: A data-mining approach to associating MISR smoke plume heights with MODIS fire measurements, Remote Sens. Environ., 107, 138–148, 2007.

ACPD
12, 19209–19241, 2012

Raffuse, S. M., Craig, K. J., Larkin, N. K., Strand, T. T., Sullivan, D. C., Wheeler, N. J. M., and Solomon, R.: An Evaluation of Modeled Plume Injection Height with Satellite-Derived Observed Plume Height, Atmosphere, 3, 103–123, doi:10.3390/atmos3010103, 2012.

Roberts, G. J. and Wooster, M. J.: Fire Detection and Fire Characterization Over Africa Using Meteosat SEVIRI, IEEE, Transactions on Geoscience and Remote Sensing, 46, 1200–1218, doi:10.1109/TGRS.2008.915751, 2008.

Roberts, G., Wooster, M. J., and Lagoudakis, E.: Annual and diurnal african biomass burning temporal dynamics, Biogeosciences, 6, 849–866, doi:10.5194/bg-6-849-2009, 2009.

Sofiev, M., Ermakova, T., and Vankevich, R.: Evaluation of the smoke-injection height from wild-land fires using remote-sensing data, Atmos. Chem. Phys., 12, 1995–2006, doi:10.5194/acp-12-1995-2012, 2012.

Sofiev, M., Siljamo, P., Valkama, I., Ilvonen, M., and Kukkonen, J.: A dispersion modelling system SILAM and its evaluation against ETEX data, Atmos. Environ., 40, 674–685, doi:10.1016/j.atmosenv.2005.09.069, 2006.

Sofiev, M., Vankevich, R., Lotjonen, M., Prank, M., Petukhov, V., Ermakova, T., Koskinen, J., and Kukkonen, J.: An operational system for the assimilation of the satellite information on wild-land fires for the needs of air quality modelling and forecasting, Atmos. Chem. Phys., 9, 6833–6847, doi:10.5194/acp-9-6833-2009, 2009.

Sukhinin, A. I., Conard, S. G., McRae, D. J., Ivanova, G. A., Tsvetkov, P. A., Bychkov, V. A., and Slinkina, O. A.: Remote Sensing of Fire Intensity and Burn Severity in Forests of Central Siberia, in: Contemporary Problems of Earth Remote Sensing from Space, available at: http://www.iki.rssi.ru/earth/ppt2005/sukhinin.pdf, last access: 31 July 2012, Space Research Institute RAS, Moscow, 2005.

Val Martin, M., Logan, J. A., Kahn, R. A., Leung, F.-Y., Nelson, D. L., and Diner, D. J.: Smoke injection heights from fires in North America: analysis of 5 years of satellite observations, Atmos. Chem. Phys., 10, 1491–1510, doi:10.5194/acp-10-1491-2010, 2010.

van der Werf, G. R., Randerson, J. T., Giglio, L., Collatz, G. J., Kasibhatla, P. S., and Arellano Jr., A. F.: Interannual variability in global biomass burning emissions from 1997 to 2004, Atmos. Chem. Phys., 6, 3423–3441, doi:10.5194/acp-6-3423-2006, 2006.

Vaughan, M. A., Powell, K. A., Kuehn, R. E., Young, S. A., Winker, D. M., Hostetler, A. C., Hunt, W. H., Liu, Z., McGill, M. J., and Getzewich, B. J.: Fully Automated Detection of Cloud and Aerosol Layers in the CALIPSO Lidar Measurements, J. Atmos. Ocean. Tech., 26, 2034–2050, doi:10.1175/2009JTECHA1228.1, 2009a.

ACPD
12, 19209–19241, 2012

Vaughan, M. A., Powell, K. A., Kuehn, R. E., Young, S. A., Winker, D. M., Hostetler, C. A., Hunt, W. H., Liu, Z., McGill, M. J., and Getzewich, B. J.: Fully Automated Detection of Cloud and Aerosol Layers in the CALIPSO Lidar Measurements, J. Atmos. Ocean. Tech., 26, 2034–2050, doi:10.1175/2009JTECHA1228.1, 2009b.

Wang, J., Christopher, S. A., Nair, U. S., Reid, J. S., Prins, E. M., Szykman, J., and Hand, J. L.: Mesoscale modeling of Central American smoke transport to the United States: 1. "Top-down" assessment of emission strength and diurnal variation impacts, J. Geophys. Res., 111, 1–21, doi:10.1029/2005JD006416, 2006.

Westphal, L. and Toon, O. B.: Simulations of Microphysical, Radiative, and Dynamical Processes in a Continental-Scale Forest Fire Smoke Plume, J. Geophys. Res., 96, 22379–22400, doi:10.1029/91JD01956, 1991.

ACPD
12, 19209–19241, 2012

Table 1. Fourier coefficients for FRP diurnal variation obtained from spectral analysis of SEVIRI data.

	a0	a1	a2	a3	b1	b2	b3
Total FRP							
Grass, 2010	1.000	−0.970	0.415	−0.143	−0.592	0.397	−0.196
Mixed, 2010	1.000	−1.288	0.631	−0.223	−0.673	0.605	−0.357
Forest, 2010	1.000	−1.180	0.587	−0.296	−0.740	0.598	−0.380
Mean FRP per pixel							
Grass, 2010	1.000	−0.214	0.140	−0.084	−0.112	0.023	−0.016
Mixed, 2010	1.000	−0.198	0.162	−0.090	−0.129	0.014	−0.003
Forest, 2010	1.000	−0.041	0.141	−0.145	−0.119	0.037	−0.021

ACPD
12, 19209–19241, 2012

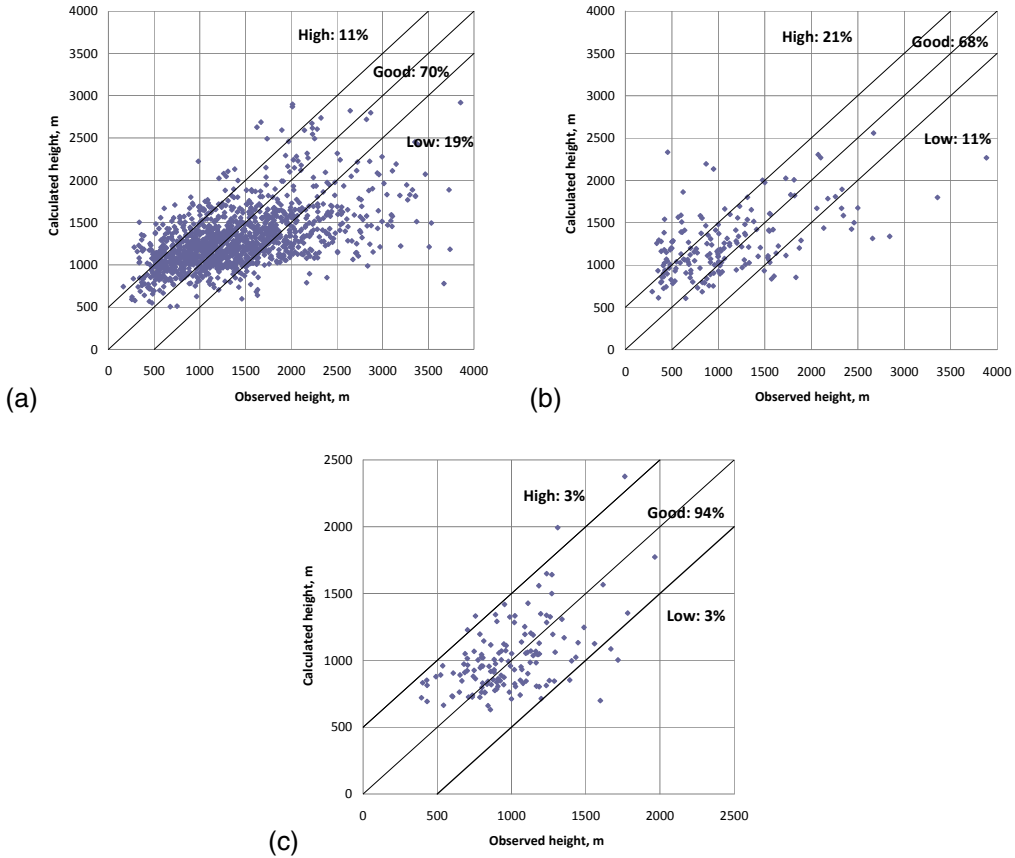

Fig. 1. Global evaluation of plume top formulations of Sofiev et al. (2012) against MISR data. Unit = [m]: **(a)** temperate and boreal fires, North America and Siberia, 2007–2009, 1321 plumes, "good quality" retrievals; **(b)** (sub-) tropical savannah, Africa, 2005–2006, 181 plumes, "good quality" retrievals; **(c)** tropical forest, Borneo, 2006, 2009, 144 plumes, "good quality" retrievals.

ACPD
12, 19209–19241, 2012

Mapping of fire smoke injection profiles

M. Sofiev et al.

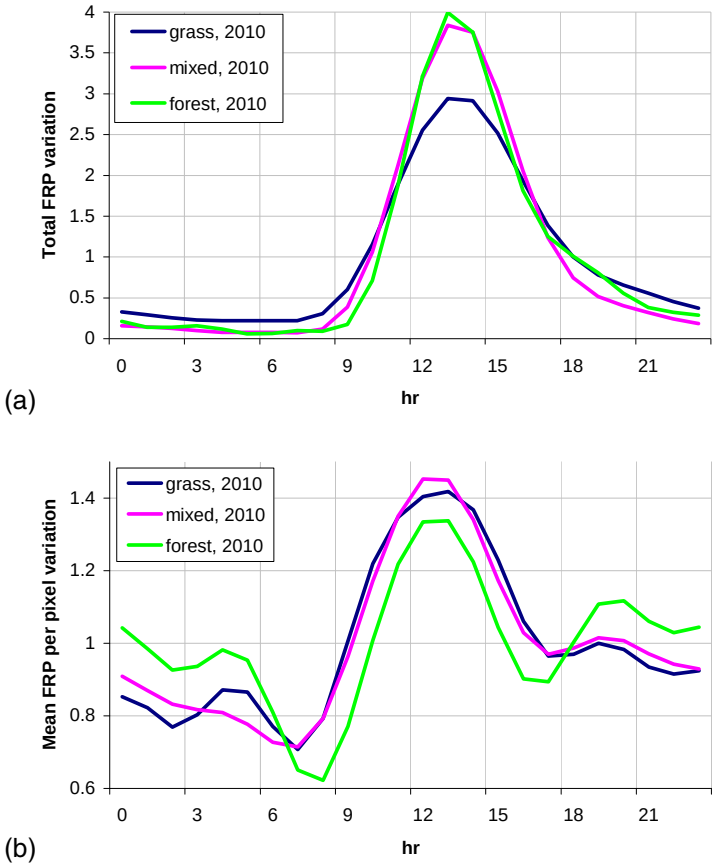

Fig. 2. Diurnal variations of **(a)** total FRP, **(b)** mean FRP per pixel. SEVIRI, mean over 2010. Relative unit.

ACPD
12, 19209–19241, 2012

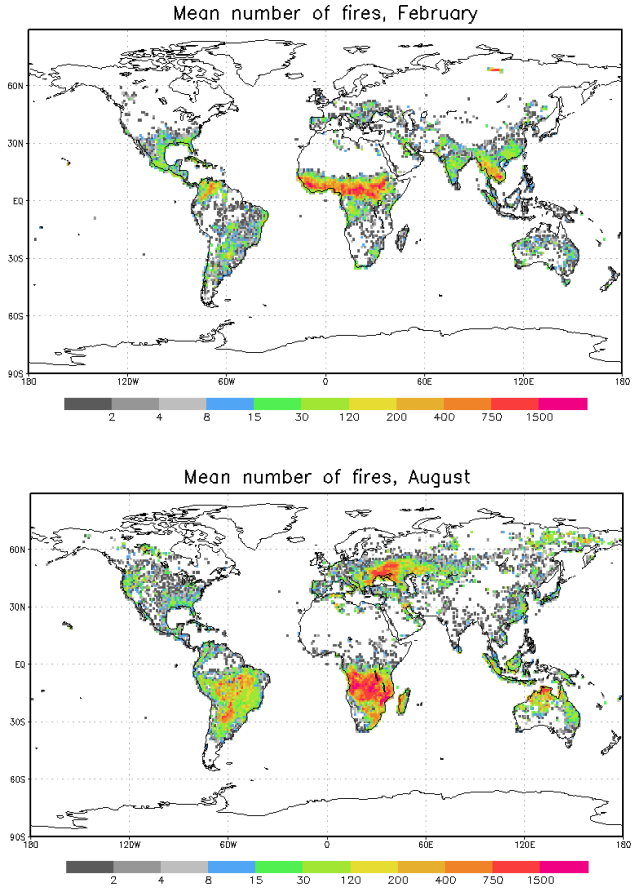

Fig. 3. Number of fires in February and August recorded by MODIS, sum of 2001 and 2008.

ACPD
12, 19209–19241, 2012

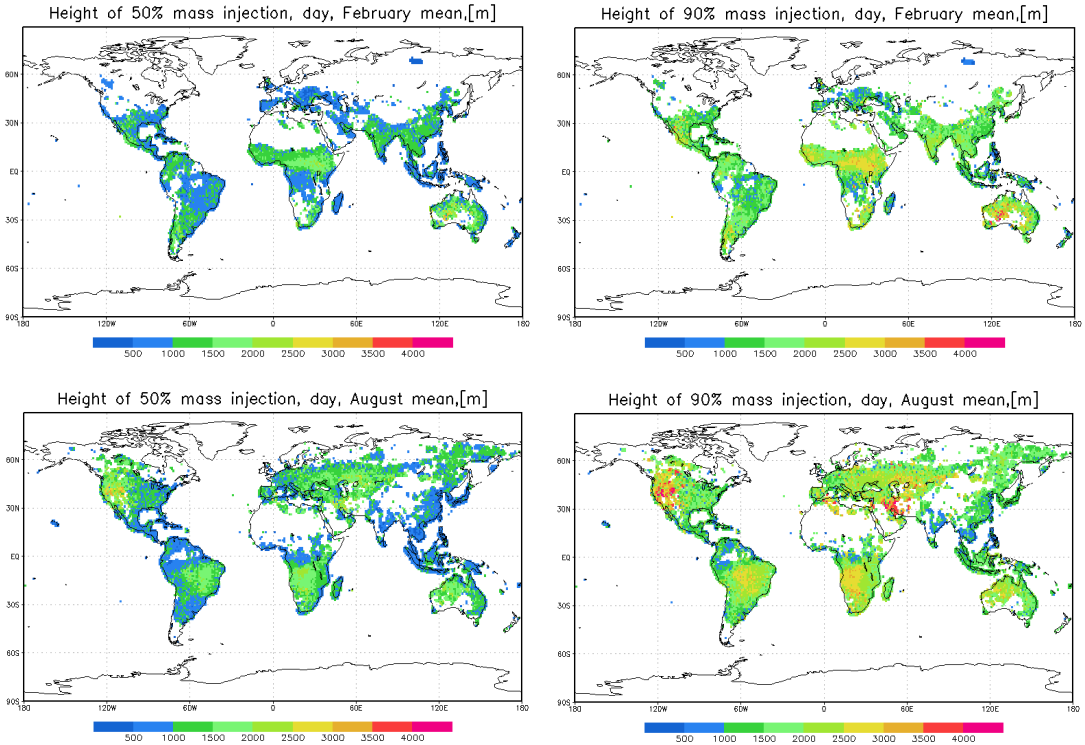

Fig. 4. Injection top height for 50 % (left) and 90 % (right) of mass for February (top) and August (bottom). Daytime. Unit = [m].

ACPD
12, 19209–19241, 2012

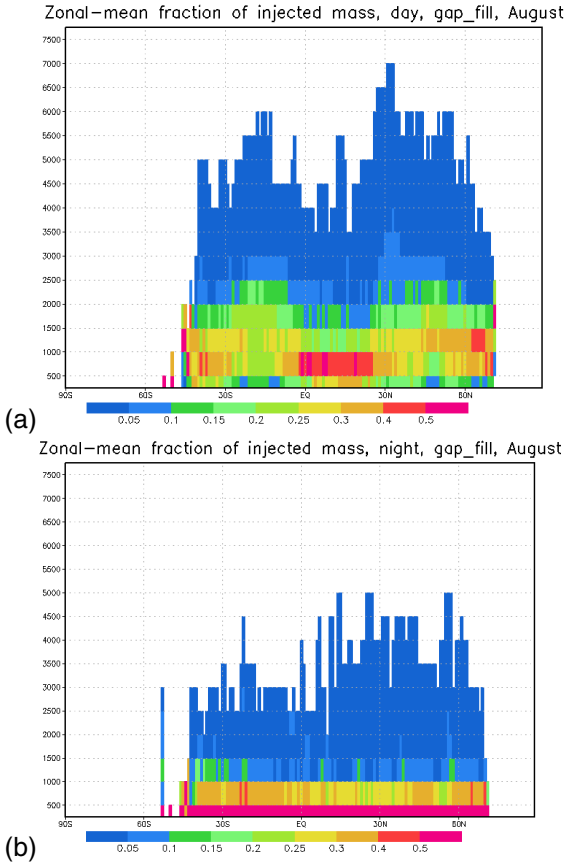

Fig. 5. Zonal average of the vertical injection profile, August: panel **(a)** daytime; panel **(b)** nighttime.

ACPD
12, 19209–19241, 2012

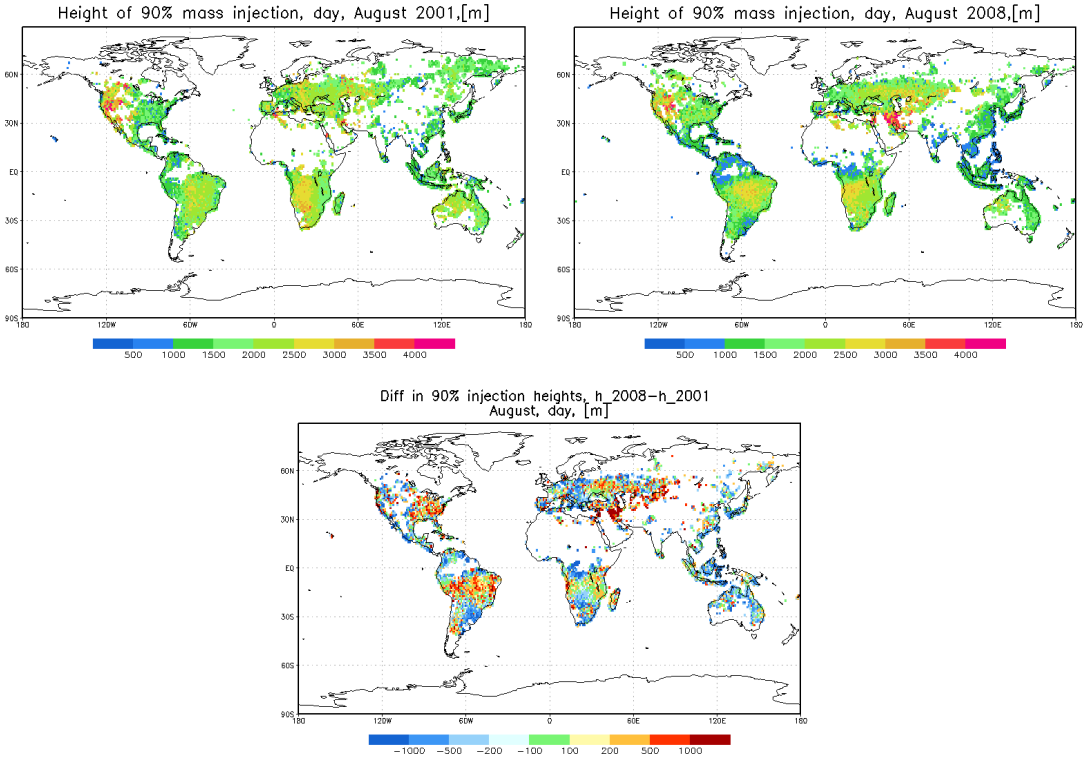

Fig. 6. Injection top height for the 90th percentile of injection profile for 2001, 2008, and difference between them. Daytime. Unit = [m].

ACPD
12, 19209–19241, 2012

Mapping of fire smoke injection profiles

M. Sofiev et al.

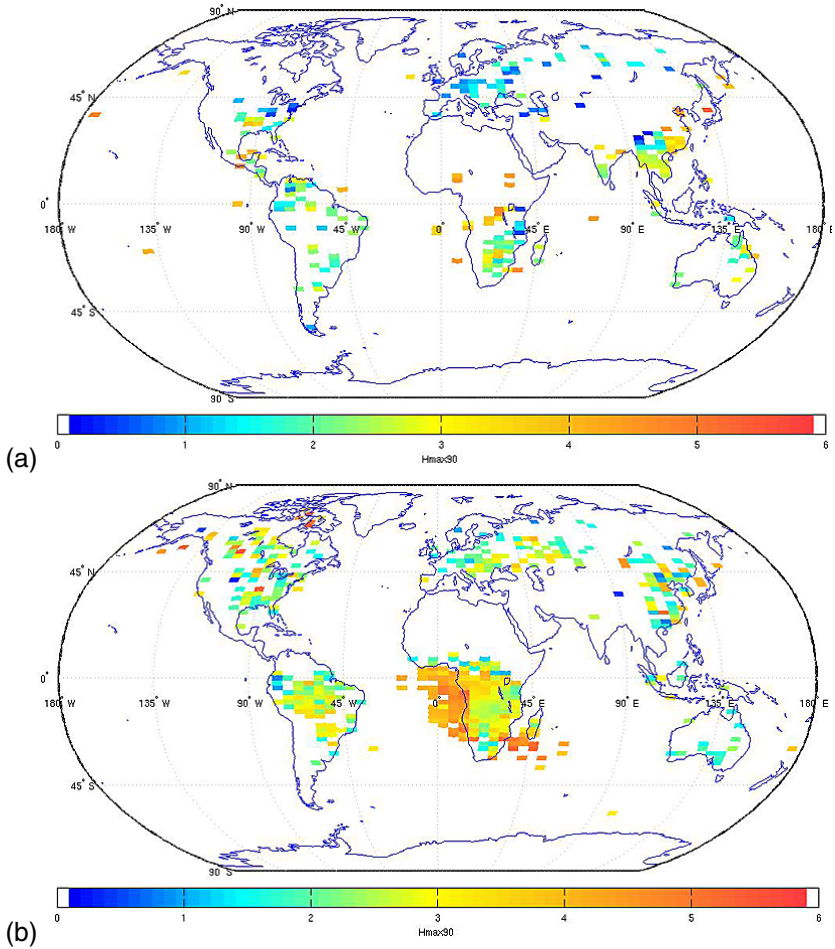

Fig. 7. The 90th percentile of the aerosol profiles observed by CALIOP lidar in 2008. Panel **(a)** – February, panel **(b)** – August. Daytime. Unit: [km].

ACPD
12, 19209–19241, 2012

Mapping of fire smoke injection profiles

M. Sofiev et al.

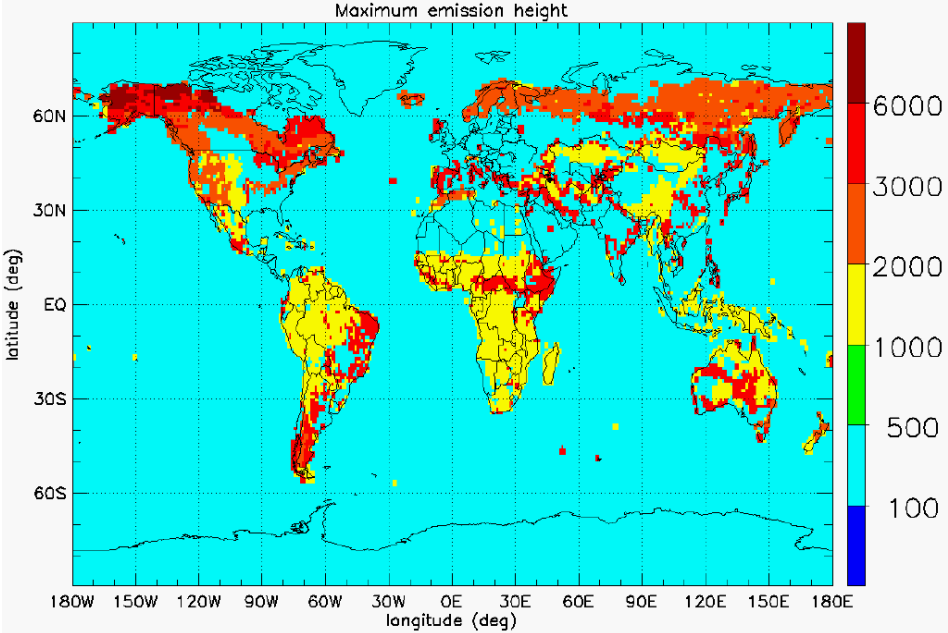

Fig. 8. Map of the plume top recommended by Dentener et al. (2006). Unit = [m]. Adopted from the online paper version.

ACPD
12, 19209–19241, 2012